communications physics

ARTICLE

https://doi.org/10.1038/s42005-021-00727-9 OPEN

Matryoshka phonon twinning in α-GaN

Bin Wei [1,2,3], Qingan Cai[3], Qiyang Sun[3], Yaokun Su [4], Ayman H. Said[5], Douglas L. Abernathy [6], Jiawang Hong [2,7]✉ & Chen Li [3,4,7]✉

Understanding lattice dynamics is crucial for effective thermal management in electronic devices because phonons dominate thermal transport in most semiconductors. α-GaN has become a focus of interest as one of the most important third-generation power semiconductors, however, the knowledge on its phonon dynamics remains limited. Here we show a Matryoshka phonon dispersion of α-GaN with the complementary inelastic X-ray and neutron scattering techniques and the first-principles calculations. Such Matryoshka twinning throughout the basal plane of the reciprocal space is demonstrated to amplify the anharmonicity of the related phonons through creating abundant three-phonon scattering channels and cutting the lifetime of affected modes by more than 50%. Such phonon topology contributes to reducing the in-plane thermal transport, thus the anisotropic thermal conductivity of α-GaN. The results not only have implications for engineering the thermal performance of α-GaN, but also offer valuable insights on the role of anomalous phonon topology in thermal transport of other technically semiconductors.

[1] Henan Key Laboratory of Materials on Deep-Earth Engineering, School of Materials Science and Engineering, Henan Polytechnic University, Jiaozuo, China. [2] School of Aerospace Engineering, Beijing Institute of Technology, Beijing, China. [3] Department of Mechanical Engineering, University of California, Riverside, CA, USA. [4] Materials Science and Engineering, University of California, Riverside, CA, USA. [5] Advanced Photon Source, Argonne National Laboratory, Lemont, IL, USA. [6] Neutron Scattering Division, Oak Ridge National Laboratory, Oak Ridge, TN, USA. [7] These authors jointly supervised this work: Jiawang Hong, Chen Li. ✉email: hongjw@bit.edu.cn; chenli@ucr.edu

Gallium nitride (GaN), one of the most important third-generation power semiconductors, excels in power density and high-temperature stability due to its wide bandgap and high thermal conductivity[1–4] (230 W m^{-1} K^{-1} at room temperature has been reported[5–8]), among many other favorable properties. To further miniaturize high-power electronics[4], great efforts have been devoted to studying the thermodynamics of α-GaN (wurtzite structure, Supplementary Fig. 1a and Supplementary Note 1 in Supplementary Information). However, the knowledge on its phonon dynamics remains limited, with key questions yet to be answered. For example, existing experimental measurements of the phonon dispersion relation of α-GaN are limited to ambient conditions, and the phonon scattering processes and the temperature effects are mostly unexplored[9,10]. Moreover, the anisotropic thermal transport of α-GaN along *a*-(in-plane) and *c*-axis (out-of-plane) directions remains controversial due to the challenges in transport measurements[7,11–18] and calculations[3,19–21]. Therefore, a more comprehensive understanding of the phonon dynamics is pivotal to investigating the thermal transport and other thermodynamics properties of GaN.

Engineering of phonon topology is one of the main strategies to manipulate thermal properties through phonon engineering besides doping[22], creating solid solution[23], isotopic engineering[24], and nanostructuring[25]. Many novel properties, such as low thermal conductivity[26–28], negative thermal expansion[29], and anomalous phase transitions[30], can be attributed to exotic phonon dispersion topology, e.g., crossing/anti-crossing behaviors[31,32], bunched acoustic phonon[33], and dispersion waterfall[34]. Recently, local phonon dispersion nesting behaviors have been shown to augment acoustic-optical three-phonon scattering channels, amplify anharmonicity, and suppress lattice thermal transport[35,36].

Here we report an in-plane Matryoshka-like phonon dispersion twinning, in which the optical and the acoustic phonon dispersions are like nesting dolls (Supplementary Fig. 2 and Supplementary Note 2). Such behavior is observed in α-GaN single crystals by both inelastic X-ray scattering (IXS) and inelastic neutron scattering (INS), and is confirmed by first principles calculations. The Matryoshka phonon twinning provides a great magnitude of acoustic-optical scattering channels and contributes to the reduction of the in-plane thermal conductivity, leading to the anisotropic thermal conductivity of α-GaN. This result is supported by the phonon lifetime measured through scattering linewidths and provides valuable insights into phonon topology engineering for thermal management.

Results and discussion

Matryoshka phonon twinning behavior in α-GaN. The phonon dispersions of α-GaN were measured by IXS below the phonon gap around 45 meV, as shown in Fig. 1a for 300 K (the dispersion measurements at 50 and 175 K can be found in Supplementary Fig. 3 and Supplementary Note 3). The measurements are in excellent agreement with first principles calculations and previous IXS results[9]. Most importantly, two parallel sections were found along Γ-M and Γ-K directions in the Brillouin zone (BZ), showing dispersion nesting behavior[35]: the near-constant energy difference is around 16 meV along Γ-M direction, while it is around 15 meV along Γ-K direction. The upper nested branch consists of low-energy optical (LEO) phonons in the lower **q** range and longitudinal acoustic (LA) phonons in the higher **q** range (referred to as the "Arc" branch in the following text), while the lower nested branch is one of the transverse acoustic branches (TA_2). Figure 1b–e show how the TA_2 and the Arc branches track each other with momentum transfer at 300 K (Other phonon branch evolutions and the temperature dependence of some optical phonons are shown respectively in Supplementary Figs. 4, 5 and Supplementary Note 3). It can be clearly observed that, along both Γ-M and Γ-K directions, the energies of these phonon modes exhibit similar dispersive behaviors with increasing **q**, leading to a nearly parallel section between the branches.

An INS experiment was performed to measure the full phonon lattice dynamics in the reciprocal space to complement the IXS data, which only cover selected high symmetry directions. The acquired dynamical susceptibility, $\chi''(\mathbf{Q}, E)$, is shown in Fig. 2 as two-dimension slices along Γ-M, Γ-K, and Γ-A directions at 14 (Fig. 2a, d, g) and 300 K (Fig. 2b, e, h), overlaid with the first principles phonon dispersion calculation. The $\chi''(\mathbf{Q}, E)$ calculations (Fig. 2c, f, i) based on first-principle phonon eigenvectors agree well with the INS measurements (Fig. 2b, e, h). The nesting behavior of the TA_2 and the Arc branches can be clearly observed along Γ-M direction in both the experimental and the calculated $\chi''(\mathbf{Q}, E)$. The nesting behavior of the TA_2 and the Arc branches can also be observed along Γ-K, although the intensity of $\chi''(\mathbf{Q}, E)$ is weaker due to the scattering structure factor.

Jointly analyzing the IXS and INS results, it is remarkable that the phonon dispersion nesting behavior is exhibited throughout the basal plane in the BZ of α-GaN (Supplementary Fig. 1b and Supplementary Note 1), as visualized by the volume and cross-section views of the measured $\chi''(\mathbf{Q}, E)$ at 300 K in Fig. 3a–d (the results at 14 K are shown in Supplementary Fig. 6 and Supplementary Note 4). Similar to the phonons along the high symmetry directions in Fig. 2, the phonons along the non-high symmetry directions exhibit similar nesting behavior (additional cuts and visual angles can be found in Supplementary Fig. 7 and Supplementary Note 4). Such phenomenon can be vividly illustrated by the phonon dispersion surfaces in Fig. 3e from the first principles calculation (also shown by the calculated phonon dispersion in Supplementary Fig. 8 and Supplementary Note 5). In the basal plane of the reciprocal space, the nested TA_2 and Arc phonon dispersion surfaces are similarly cone-shaped and nest together in a Matryoshka-like twinning behavior (Fig. 3e). Such Matryoshka twinning is reflected by both the first principles calculations and INS projection contours (Fig. 3f, g and Supplementary Fig. 8 and Supplementary Note 5). Similar to the case of CuCl where the phonon nesting arises from the ionic radius mismatch[36], the large ionic radius mismatch of N (0.75 Å) and Ga (1.62 Å) atoms are also responsible for the Matryoshka phonon twinning in α-GaN. In addition, such Matryoshka behavior may also be attributed to the two [GaN4] tetrahedrons along *c*-axis in the crystal structure. Unlike the monolayer GaN[3], the double tetrahedral units along *c*-axis induce the TA branch folding from the zone boundary (A-point), and thus lead to a low-energy of the Arc at Γ-point. Such Matryoshka twinning may provide vast three-phonon scattering channels in α-GaN by reducing the momentum transfer constraint, thus expanding the phonon scattering phase space. For example, in a three-phonon emission process where one phonon mode on the Arc branch ($\mathbf{q}_{Arc}$, ω_{Arc}) decays into two phonon modes ($\mathbf{q}_1$, ω_1) and ($\mathbf{q}_2$, ω_2), for the mode ($\mathbf{q}_1$, ω_1) on the Arc branch near Γ point, we can always find a TA_2 mode ($\mathbf{q}_2 = \mathbf{q}_{Arc} - \mathbf{q}_1$, $\omega_1 = \omega_{Arc} - \omega_1$) in the basal plane that enables such scattering (Supplementary Fig. 9 and Supplementary Note 6). This scattering behavior is consistent with recent report of weighted phonon scattering space in α-GaN, which shows the emission process is significantly larger than that of the absorption process in the energy range from 20 to 40 meV (~5 THz to ~10 THz), (Supplementary Fig. 10a and Supplementary Note 7)[6] in line with the energy range of the Arch branch in the Matryoshka twinning.

The impact of Matryoshka phonon twinning on the anharmonic scattering rate. Phonon linewidths of α-GaN at 300 K were extracted from IXS by de-convoluting the energy and momentum resolution functions, INS by de-convoluting the

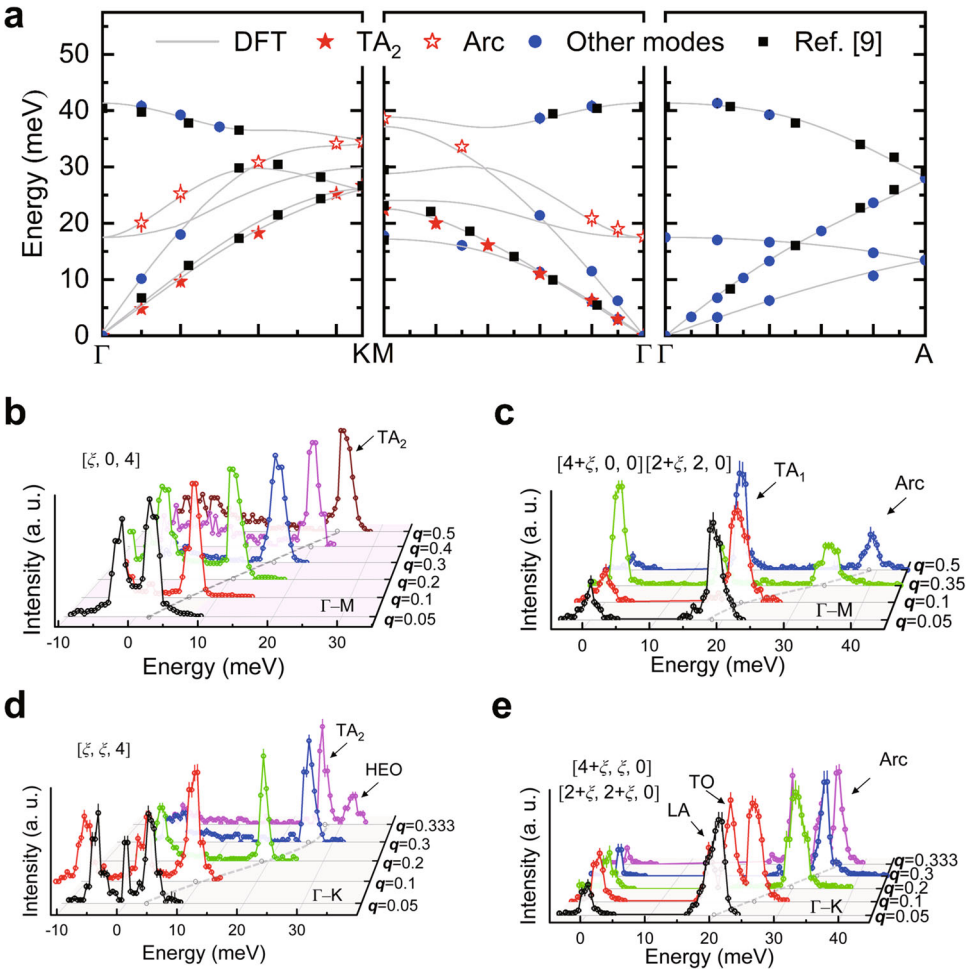

Fig. 1 Phonon dispersion nesting observed by inelastic X-ray scattering (IXS) measurements in α-GaN. a The measured phonon dispersion of α-GaN by IXS at 300 K overlays on the calculation (DFT) gray lines). Along Γ–M and Γ–K, the second transverse acoustic branch (TA_2) (solid stars) and the higher nested branch (Arc) (hollow stars) jointly show the nesting behavior. The energy of the Arc branch at Γ point was measured by Raman spectroscopy. The error bars are the uncertainties of a least-squares fitting result from the damped-harmonic-oscillator model and comparable to or smaller than the data point symbols. Black squares are the IXS results from ref. [9]. **b**–**e** The measured phonon spectra evolution of TA_2 and Arc branches with increasing momentum **q** along Γ–M and Γ–K at 300 K (reciprocal lattice units—r.l.u.). The phonon mode trends are reflected by the gray dash line with the peak centers labeled by circles. TA_2 branches were measured in the (004) zone along scattering wavevector $\mathbf{Q} = [\xi, 0, 4]$ (Γ–M) and $\mathbf{Q} = [\xi, \xi, 4]$ (Γ–K) respectively, while Arc branches were measured in the (400) (the transverse optical mode, TO) and (220) (the longitudinal acoustic mode, LA) zones along scattering wavevectors $\mathbf{Q} = [4 + \xi, 0, 0]$ and $\mathbf{Q} = [2 + \xi, 2, 0]$ (Γ–M), and $\mathbf{Q} = [4 + \xi, \xi, 0]$ and $\mathbf{Q} = [2 + \xi, 2, 0]$ (Γ–K) respectively. The peak intensity at each momentum **q** point was rescaled.

energy resolution function, and Raman spectroscopy (at Γ-point) without considering the instrument resolution. The INS results are moderately in consistent with the IXS measurement (Supplementary Fig. 10b and Supplementary Note 7). The Raman spectroscopy (https://chenwli.com/facilites/) gives a linewidth of 0.8 meV for the Arc branch at the Γ-point (Fig. 4d), where the linewidth is also found to be narrow by INS. Although the measured phonon linewidths vary between different techniques because of their different resolution functions, it is reasonable to compare them within one technique to quantify the linewidth difference between the phonons related to Matryoshka twinning and other branches. Phonon linewidth is proportional to the total scattering rate from all processes[35,37] and dominated by anharmonic phonon–phonon interactions in α-GaN. As shown in Fig. 4a, while the linewidths of most phonon modes are between 0.5 and 1.5 meV, the linewidths of the phonon modes on the TA_2 and the Arc branches are much broader and double of some other phonon modes. These large linewidths indicate that the nested phonons are scattered more strongly than the others, leading to the phonon lifetime of nested modes is cut by more than 50%. In Fig. 4b, c, it is found that the linewidths of phonon modes on the TA_2 and Arc branches (low-**q** in TO and high-**q** in LA) are much larger than those on the high energy optical (HEO) branch along Γ-M direction and those on the HEO and LEO branches along Γ-A direction. The anharmonic phonon scattering rate is expressed as[38]

$$\begin{aligned}\tau_{\mathbf{q}s}^{-1} &= 2\Gamma_{\mathbf{q}s} = \frac{36\pi}{\hbar^2}\sum_{q_1,q_2,q_3}|V(\mathbf{q},\mathbf{q}_1,\mathbf{q}_2,s,s_1,s_2)|^2 \\ &\times (n_1+n_2+1)\Big\{\delta(\omega_1+\omega_2-\omega_{\mathbf{q}s})-\delta(\omega_1+\omega_2+\omega_{\mathbf{q}s})\Big\} \\ &+(n_2-n_1)\delta(\omega_1-\omega_2-\omega_{\mathbf{q}s})-\delta(\omega_1-\omega_2+\omega_{\mathbf{q}s})\end{aligned} \quad (1)$$

where V is the third-order interatomic potential, ω_{qs} is the phonon frequency of the phonon mode of wavevector **q** and branch index s, and n is Bose occupation. This anharmonic scattering rate is determined by both the third-order interatomic potentials and the phonon scattering phase space: the former represents the scattering strength, and the latter represents the phase space of

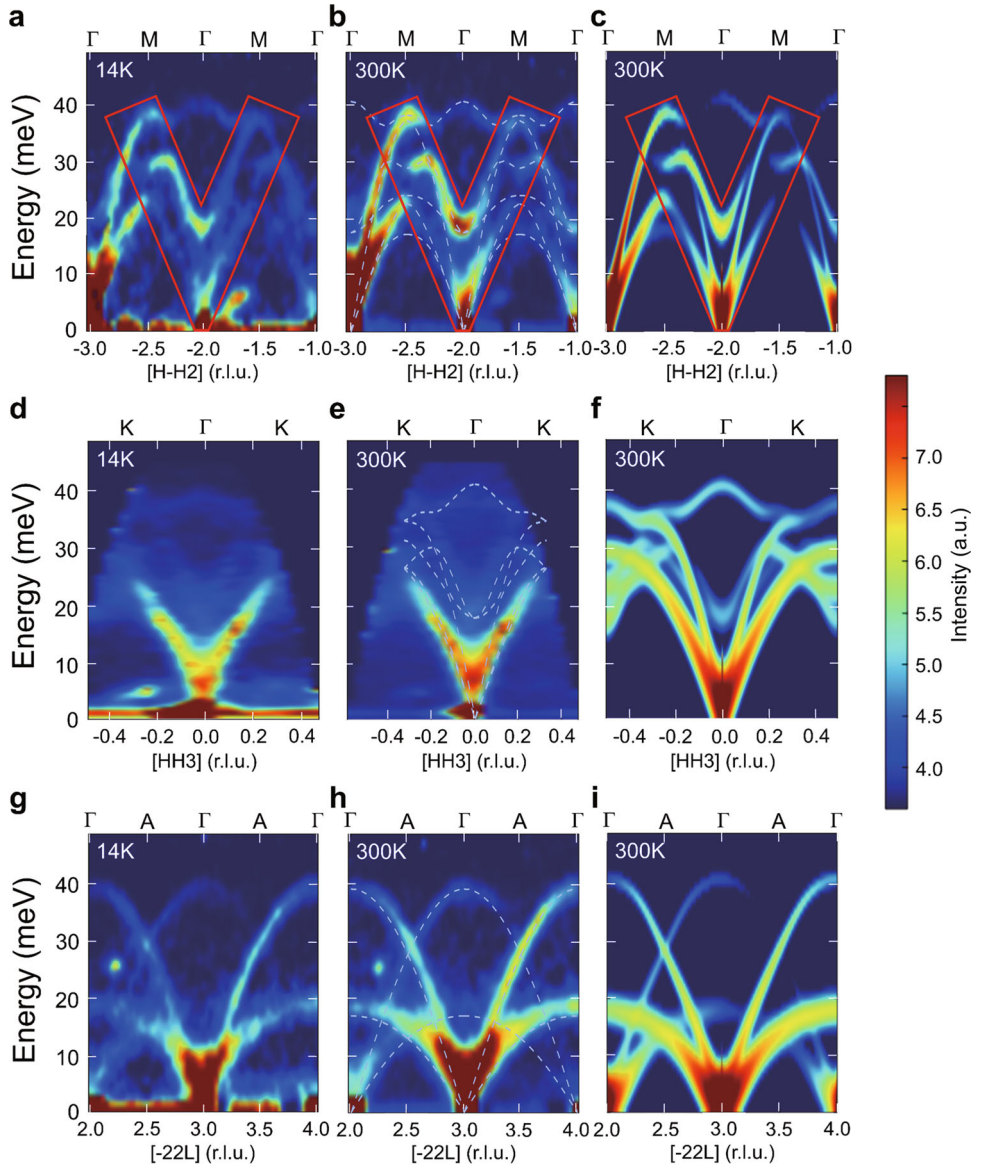

Fig. 2 Phonon dispersion nesting observed in the dynamical susceptibility $\chi''(\mathbf{Q}, E)$ from inelastic neutron scattering (INS) measurements. **a**, **b**, **c** are the $\chi''(\mathbf{Q}, E)$ for scattering wavevector **Q** along [H, -H, 2] (r.l.u.). **d**, **e**, **f** are the results along [H, H, 3]. **a**, **d** are the results at 14 K, (**b**, **e**) are the results at 300 K overlaid with the calculated phonon dispersion, and (**c**, **f**) are the calculated χ'' (**Q**, *E*) at 300 K. The parallel sections were marked by the red boxes. **g**, **h**, **i** are the results along [−2, 2, L]. Small dots ((−2, 2, 2) to (−1.5, 1.5, 2) along Γ–M and around (−2, 2, 2.2) along Γ–A) in the measured $\chi''(\mathbf{Q}, E)$ are multiple scattering artifacts. Color bar indicates the phonon intensities plotted on a logarithmic scale.

available scattering channels[39]. The large linewidths of the phonons involved in the Matryoshka twinning suggest that such behavior significantly promotes three-phonon scatterings in α-GaN.

To elucidate the anharmonicity of the phonon modes on the Arc branch in α-GaN, the evolution of the phonon energy at $\mathbf{q} = 0.1$ along Γ-M direction was fitted over a wide temperature range with the following expression[40]

$$\omega_A(T) = \omega(0) - A\left(1 + 2/\left(e^{\frac{\hbar\omega(0)}{2k_BT}} - 1\right)\right) \quad (2)$$

where A and $\omega(0)$ are fitting constants, and $\omega_A(T)$ is the temperature-dependent phonon energy. The result in Fig. 5a shows a moderate anharmonicity below the Debye temperature (~636 K)[11], supported by the moderate difference between experimental isobaric[41] and calculated volumetric mode Grüneisen parameters[42] (Fig. 5b), see the details in Supplementary Note 8. Additionally, the frozen phonon potential for the phonon mode on the Arc branch at $\mathbf{q} = 0.1$ along Γ-M direction (Fig. 5c) only slightly departs from the harmonic behavior, indicating moderate anharmonicity (the phonon eigenvectors are shown in the insert in Fig. 5c). Considering such moderate anharmonicity, it is confirmed that the large linewidths of the phonon modes in the TA_2 and Arc branches are dominated by the enlarged scattering phase space from the vast scattering channels induced by the Matryoshka twinning.

The impact of Matryoshka phonon twinning on the anisotropic thermal conductivity. The anisotropic thermal conductivity of α-GaN recently attracted intensive attention because it is critical for heat management in power electronics, where α-GaN is a key component. However, the answer remains controversial: due to the difficulty of the anisotropic thermal conductivity measurement[7], previous theoretical calculations reported that the in-plane thermal conductivity is greater than the out-of-plane one while others showed

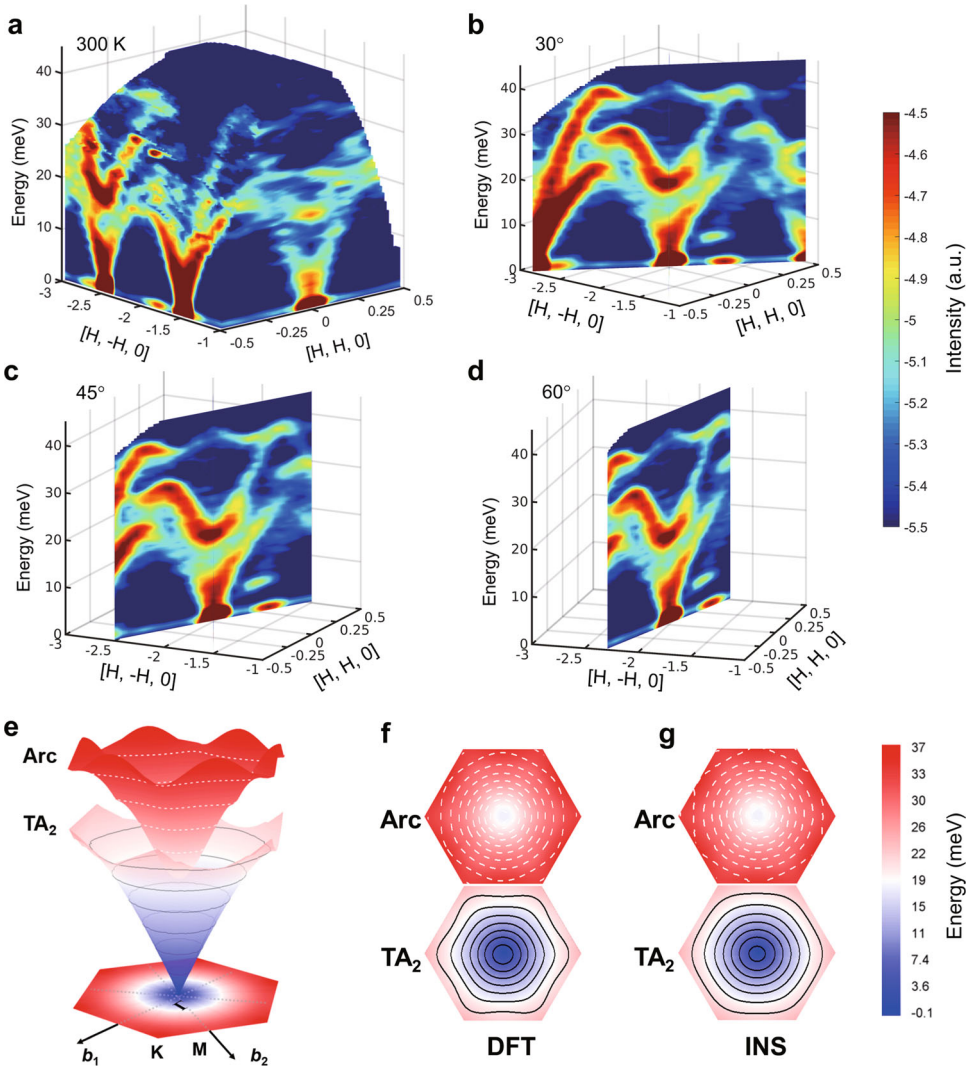

Fig. 3 The in-plane Matryoshka-like dispersion behavior shown by inelastic neutron scattering (INS) and first principles calculations (DFT). a Volumetric view of the measured dynamical susceptibility $\chi''(\mathbf{Q}, E)$ throughout the basal plane in the Brillouin zone at 300 K. **b**, **c**, **d** Cuts at 30°, 45°, and 60° from the [H -H 0] direction respectively. Color bar indicates the intensities plotted on a logarithmic scale. **e** Side view of the second transverse acoustic (TA_2) and the higher nested (Arc) branches from first principles calculation, illustrating the huge parallel region between the two surfaces. The bottom panel indicates the projection on the basal plane. $\mathbf{b}_1$ and $\mathbf{b}_2$ are the reciprocal space vectors. **f**, **g** are the projection contours of the TA_2 and Arc branches on the basal plane from DFT and INS results, respectively. The white dash line and the black solid line indicate the Arc and TA_2 phonon surfaces' energy contours, respectively. The energy difference between the contours of the Arc and TA_2 phonon surfaces is 2.5 meV. The color scale indicates the phonon surface energies.

opposite results[3,5,6,19,20]. Among these reports, three recent theoretical calculations showed that the in-plane thermal conductivity is lower. Qin et al. reported that the in-plane and the out-of-plane thermal conductivities are 280 and 325 W m^{-1} K^{-1}, with an anisotropy ratio of 14%[3]. Wu et al.[19] and Yang et al.[20] reported that the in-plane and the out-of-plane thermal conductivities are 228 and 260 W m^{-1} K^{-1}, with an anisotropy ratio of 12%. These two reports both show good agreement with the measured value around 230 W m^{-1} K^{-1}[8] and thus provide relatively reliable reference for the anisotropy of the thermal conductivity of α-GaN.

Understanding the temperature dependence of the anisotropic thermal conductivity requires considering both changes of the anharmonic phonon scattering rates and phonon dispersion/group velocities[26], as shown in the following equation:

$$\kappa = \sum_{\mathbf{q}s} C_{\mathbf{q}s} v_{\mathbf{q}s}^2 \tau_{\mathbf{q}s} \quad (3)$$

where $C_{\mathbf{q}s}$ is the heat capacity, $v_{\mathbf{q}s}$ the group velocity, and $\tau_{\mathbf{q}s}$ the phonon lifetime of wavevector $\mathbf{q}$ and branch index s. Usually, acoustic and low-energy optical phonons contribute more to the thermal conductivity than other less dispersive modes so only their contribution is considered here. The temperature-dependent acoustic phonon group velocities were extracted from the measured phonon spectra (Fig. 2), as shown in Table 1. The acoustic phonon group velocities along the out-of-plane (Γ-A) direction are slightly larger than those along the in-plane (Γ-M and Γ-K) directions. For the LA (TA_2) branch, the phonon group velocities along Γ-A are 1%, 1.7%, and 0.8% (3.7%, 3%, and 4%) larger than those along Γ-M at 14, 50, and 300 K, respectively. This behavior indicates that the anisotropy of acoustic phonon group velocity is minor and may not induce a sizable thermal conductivity anisotropy in α-GaN.

As discussed previously, the effects of in-plane Matryoshka twinning on the scattering rates of in-plane phonons are significant, shown by the anomalously large linewidths of the modes involved at 300 K. In Fig. 4, the Arc, TA_2, and other in-plane branches have phonon linewidths around 2.3, 2, and 1.3 meV, respectively. The out-

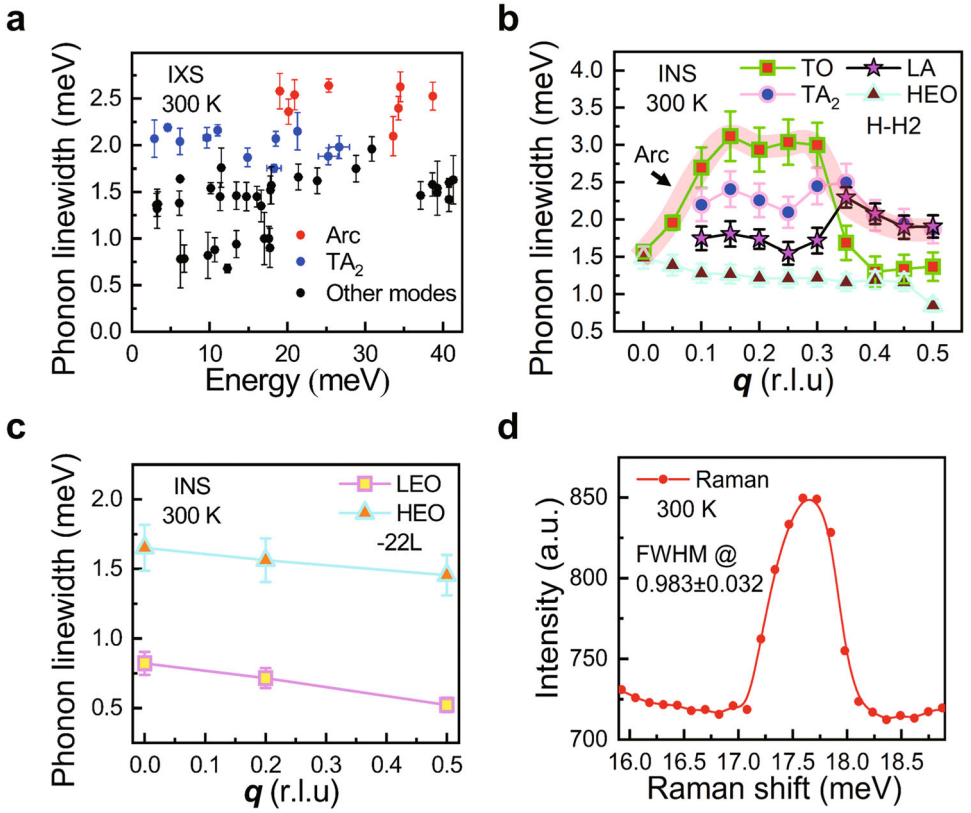

Fig. 4 Phonon linewidths of the low-energy modes in α-GaN. a Linewidths of phonon modes from the inelastic X-ray scattering (IXS) data at 300 K. **b**, **c** Phonon linewidths of the higher nested branch (Arc, composed of the low momentum **q** transverse optical, TO and the high momentum **q** longitudinal acoustic, LA modes) (light pink shadow), the second transverse acoustic (TA_2), and the high energy optical (HEO) modes along Γ–M and phonon linewidths of the HEO and the low-energy optical (LEO) modes along Γ–A from the inelastic neutron scattering (INS) data at 300 K, respectively. **d** Phonon mode and the linewidth (full width at half maximum, FWHM) of the Arc at Γ point from Raman data at 300 K. Raman spectroscopy only provides information on Raman-active modes at zone centers (Γ point). The error bars are the uncertainties of a least-squares fitting result from the damped-harmonic-oscillator model.

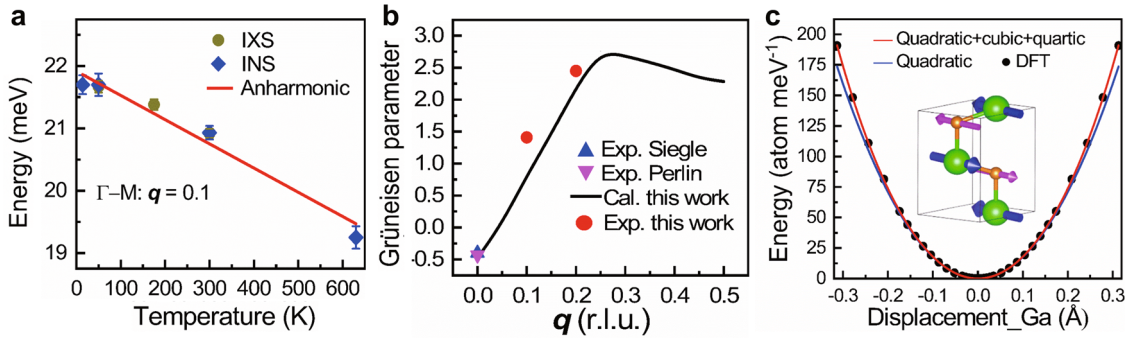

Fig. 5 Anharmonicity of the optical mode in the higher nested branch (Arc) at momentum q = 0.1 along Γ–M in α-GaN. a Temperature dependence of phonon energy. Data were obtained from both inelastic X-ray scattering (IXS) and inelastic neutron scattering (INS) measurements. The lines show the fitting of the data points by Eq. (2). The error bars are the uncertainties of a least-squares fitting result from the damped-harmonic-oscillator model. **b** The experimental (Exp.) mode Grüneisen parameters of the phonon modes on the Arc branch, compared with the first principles calculations (Cal.) along Γ–M. The blue triangle and the pink inverted triangle are the data from the Raman measurements reported by Siegle et al.[51] and Perlin et al.[52] respectively. **c** The frozen phonon potential of the Arc at **q** = 0.1 along Γ–M corresponding to the displacement of Ga along *b*-axis. Inset indicates the corresponding vibration mode, where the green balls represent Ga atoms and orange balls represent N atoms. The vectors indicate the direction of the displacement of the corresponding atoms.

of-plane HEO and other branches (LEO, TA, and LA) have phonon linewidths around 1.5 and 1.2 meV, respectively. Considering the instrument resolution, the phonon lifetimes of TA_2 and the high-**q** part of LA are estimated to be <50% of their counterparts in the basal plane. Assuming similar group velocities for in-plane and out-of-plane phonon branches and using Eq. (3), the thermal conductivity contribution by TA_1/LA, TA_2, and Arc (TO) branches is roughly estimated to be 8%, 40%, and 48% lower, respectively, along the in-plane direction than the out-of-plane direction. The Matryoshka twinning amplifies the acoustic-optical three-phonon scattering in α-GaN and thus reduces the in-plane thermal conductivity, especially at temperatures above the Debye temperature, when the lattice thermal

Table 1 Group velocity (v_g) of the longitudinal acoustic (LA) and the second transverse acoustic (TA_2) phonons along the high symmetry directions from experimental data.

Direction	Temperature (K)	LA v_g (m s^{-1})	TA_2
Γ–M [100]	14	8319	4142
	50	8149	4008
	300	8015	3894
	DFT	7909	4088
Γ–K [110]	50	7521	3768
	300	7363	3466
	DFT	7465	3941
Γ–A [001]	14	8403	4303
	50	8290	4135
	300	8087	4062
	DFT	7987	3984

Relaxed first principles (DFT) results are listed for comparison.

transport is dominated by the phonon–phonon interactions. Therefore, the anisotropy of thermal conductivity is mostly a result of the twinning behavior. If such Matryoshka phonon twinning could be suppressed by phonon engineering through strain or doping, the in-plane thermal transport properties of α-GaN may potentially be enhanced for better thermal management at high temperatures.

Conclusion

Through a combination of inelastic X-ray and neutron scattering experiments and first principles calculations, a Matryoshka phonon twinning is found throughout the basal plane of the BZ in α-GaN. This phenomenon creates a vast number of three-phonon scattering channels and leads to enhanced anharmonic phonon scattering, shown by anomalously large phonon linewidths. The strong in-plane phonon scatterings due to the Matryoshka phonon twinning suppress the in-plane thermal conductivity of α-GaN and enhance the thermal transport anisotropy, while its acoustic phonon group velocities remain fairly isotropic. Amplification and suppression of such Matryoshka phonon twinning by phonon engineering could provide a valuable means to control lattice thermal transport in many related materials, such as electronic devices, thermoelectrics, and thermal barriers.

Methods

Sample preparation. High-quality GaN single crystals (un-doped, n-type, MTI Corporation https://www.mtixtl.com/GaN-C-50D025C2.aspx) used in this work were grown by the hydride vapor phase epitaxy (HVPE)-based method with low dislocation density (<1×10^7 cm^{-2}) (Supplementary Fig. 1c and Supplementary Note 1). The quality of the crystals was checked with both X-ray and neutron diffraction. The full width at half maximum (FWHM) of the X-ray diffraction peak at (002) plane is around 0.10 ± 0.02° (Supplementary Fig. 1d and Supplementary Note 1).

Inelastic scattering experiments

Inelastic X-ray scattering measurements. High-resolution IXS experiment was performed to measure the phonon dispersions of an α-GaN single crystal (250 μm thickness, the lower panel of Supplementary Fig. 1c and Supplementary Note 1) at 50, 175, and 300 K. The measurements were conducted at 30-ID-C (the High-resolution Inelastic X-ray Scattering beamline, HERIX) at the Advanced Photon Source (APS)[43,44]. The incident photon energy was ~23.7 keV with an energy resolution ΔE of 1.2 meV and a momentum resolution of 0.65 nm^{-1}. The single crystal was attached to a copper post by varnish and the copper post was mounted in a closed-cycle cryostat. The IXS measurements were accomplished at constant wavevector mode in reflection geometry. The orientation matrix was defined by using Bragg peaks at (4 0 0), (0 0 4), (0 0 5), and (2 2 0) respectively.

Inelastic neutron scattering measurements. The INS measurements were carried out on a bigger single crystal ($\varphi = 5$ cm, upper panel of Supplementary Fig. 1c and Supplementary Note 1) on the Wide Angular-Range Chopper Spectrometer, time-of-flight neutron spectrometer at the Spallation Neutron Source (SNS) at Oak Ridge National Laboratory[45]. An incident energy of $E_i = 50$ meV and a Fermi chopper frequency of 420 Hz were used to optimize instrument energy resolution. At the elastic scattering, the energy resolution is 2 meV. For INS, the [110] axis was set vertical, and scattering plane was selected to obtain both the in-plane and out-plane phonons at 14, 50, 300, and 630 K. When collecting the data, 1° step was used with a rotation range from −90° to 90° for 300 K, and 2° step was used with a rotation range from −70° to 50° for other temperatures. Because of the geometry of the substrate sample, the neutron absorption is very small when incident beam is near perpendicular to the substrate surface. The neutron absorption significantly reduces the counting statistics when incident and scattered neutron beams are near parallel to the substrate surface, but this do not affect the dispersion measurement. Data reduction was performed using the Mantid program[46]. The data were normalized by the accumulated incident neutron flux, and the detector efficiency correction was applied based on the incoherent scattering of the vanadium standard.

Scattering data processing. INS data shown in the present work were corrected for the sample temperature to obtain the dynamical susceptibility, $\chi''(\mathbf{Q}, E) = S(\mathbf{Q}, E)/[n_T(E) + 1]$, where $n_T(E)$ stands for the Bose distribution, $S(\mathbf{Q}, E)$ is the four-dimensional scattering dynamical structure factor[47]

$$S(\mathbf{Q},E) \propto \sum_s \sum_\tau \frac{1}{\omega_s} \left| \sum_d \frac{\overline{b}_d}{\sqrt{M_d}} \exp(-W_d) \exp(i\mathbf{Q}\cdot\mathbf{r}_d)(\mathbf{Q}\cdot\mathbf{e}_{ds}) \right|^2 \times \langle n_s + 1 \rangle \delta(\omega - \omega_s)\delta(\mathbf{Q} - \mathbf{q} - \tau) \quad (4)$$

where $\overline{b}_d$ is the neutron scattering length, $\mathbf{Q} = \mathbf{k} - \mathbf{k}'$ is the wavevector transfer, and $\mathbf{k}'$ and $\mathbf{k}$ are the final and incident wavevector of the scattered particle. $\mathbf{q}$ is the phonon wavevector, ω_s is the eigenvalue of the phonon corresponding to the branch index s, τ is the reciprocal lattice vector, d is the atom index in the unit cell, $\mathbf{r}_d$ is the atom position, W_d is the corresponding Debye-Waller factor, and $\mathbf{e}_{ds}$ is the phonon eigenvectors. For given $\mathbf{Q}$, the measured scattering spectra were fitted with a damped-harmonic-oscillator model[48]

$$S(\omega) = [1 + n(\omega)] \frac{1}{\pi M} \frac{\gamma\omega}{(\omega - \omega_0)^2 + (\gamma\omega)^2} \quad (5)$$

where M is the effective mass, ω_0 is the bare phonon energy in the absence of damping forces, and 2γ is a damping factor that describes the phonon scattering rates. n is the Bose distribution. The bare phonon energy and phonon linewidths were extracted by de-convoluting with both instrument energy and momentum resolution functions, the latter of which eliminates the slope effect of highly dispersive phonons on linewidths.

First principles calculations. The first principles calculations were performed based on the density functional theory as implemented in the Vienna Ab Initio Simulation Package[49]. The exchange–correlation energy was computed using the local-density approximation functional, and the projector-augmented-wave potentials were used ($4s^2 4p^1$ for Ga and $2s^2 2p^3$ for N). For plane-wave expansion in reciprocal space, we used 600 eV as the kinetic energy cutoff value. The $\mathbf{q}$-mesh was chosen as $7 \times 7 \times 5$. The convergence criteria for total energy was set to 1×10^{-8} eV, and that for atomic force was 10^{-3} eV/Å. The structure was fully relaxed and the lattice constants, $a = b = 3.188$ Å, $c = 5.190$ Å, are slightly smaller than the experimental values ($a = b = 3.191$ Å, $c = 5.191$ Å obtained from HERIX at 300 K). The phonon dispersion of α-GaN at the level of harmonic approximation was calculated using the Phonopy package[50] with $4 \times 4 \times 3$ supercell of α-GaN containing 192 atoms.

Data availability

All data needed to evaluate the conclusions in the paper are present in the paper and/or the Supplementary Figs. 1–10. Additional data related to this paper may be requested from the authors.

Received: 21 May 2021; Accepted: 16 September 2021;
Published online: 12 October 2021

References

1. Amano, H. et al. The 2018 GaN power electronics roadmap. *J. Phys. D Appl. Phys.* **51**, 163001 (2018).
2. Chung, K., Lee, C. H. & Yi, G. C. Transferable GaN layers grown on ZnO-coated graphene layers for optoelectronic devices. *Science* **330**, 655–657 (2010).
3. Qin, Z., Qin, G., Zuo, X., Xiong, Z. & Hu, M. Orbitally driven low thermal conductivity of monolayer gallium nitride (GaN) with planar honeycomb structure: a comparative study. *Nanoscale* **9**, 4295–4309 (2017).
4. Ebrahimi, K., Jones, G. F. & Fleischer, A. S. A review of data center cooling technology, operating conditions and the corresponding low-grade waste heat recovery opportunities. *Renew. Sust. Energ. Rev.* **31**, 622–638 (2014).

5. Lindsay, L., Broido, D. A., & Reinecke, T. L. Thermal conductivity and large isotope effect in GaN from first principles. *Phys. Rev. Lett.* **109**, 095901 (2012).
6. Yang, J. Y., Qin, G. & Hu, M. Nontrivial contribution of Fröhlich electron-phonon interaction to lattice thermal conductivity of wurtzite GaN. *Appl. Phys. Lett.* **109**, 242103 (2016).
7. Zheng, Q. et al. Thermal conductivity of GaN, ^{71}GaN, and SiC from 150 K to 850 K. *Phys. Rev. Materials* **3**, 014601 (2019).
8. Mion, C., Muth, J., Preble, E. & Hanser, D. Accurate dependence of gallium nitride thermal conductivity on dislocation density. *Appl. Phys. Lett.* **89**, 092123 (2006).
9. Ruf, T. et al. Phonon dispersion curves in wurtzite-structure GaN determined by inelastic x-ray scattering. *Phys. Rev. Lett.* **86**, 906 (2001).
10. Nipko, J. C. & Loong, C. K. Phonon density of states of bulk gallium nitride. *Appl. Phys. Lett.* **73**, 34–36 (1998).
11. Adachi, K. et al. Elastic constants of GaN between 10 and 305 K. *J. Appl. Phys.* **119**, 245111 (2016).
12. Shibata, H. et al. High thermal conductivity of gallium nitride (GaN) crystals grown by HVPE process. *Mater. Trans.* **48**, 2782–2786 (2007).
13. Slack, G. A., Schowalter, L. J., Morelli, D. & Freitas, J. A. Jr Some effects of oxygen impurities on AlN and GaN. *J. Cryst. Growth* **246**, 287–298 (2002).
14. Jeżowski, A. et al. Thermal conductivity of GaN crystals in 4.2-300 K range. *Solid State Commun.* **128**, 69–73 (2003).
15. Paskov, P. P., Slomski, M., Leach, J. H., Muth, J. F. & Paskova, T. Effect of Si doping on the thermal conductivity of bulk GaN at elevated temperatures-theory and experiment. *AIP Adv.* **7**, 095302 (2017).
16. Slomski, M., Paskov, P. P., Leach, J. H., Muth, J. F. & Paskova, T. Thermal conductivity of bulk GaN grown by HVPE: Effect of Si doping. *Phys. Status Solidi B* **254**, 1600713 (2017).
17. Jeżowski, A. et al. Thermal conductivity of heavily doped bulk crystals GaN: O. Free carriers contribution. *Mater. Res. Express* **2**, 085902 (2015).
18. Rounds, R. Thermal conductivity of GaN single crystals: Influence of impurities incorporated in different growth processes. *J. Appl. Phys.* **124**, 105106 (2018).
19. Wu, R., Hu, R. & Luo, X. First-principle-based full-dispersion Monte Carlo simulation of the anisotropic phonon transport in the wurtzite GaN thin film. *J. Appl. Phys.* **119**, 145706 (2016).
20. Yang, X., Feng, T. L. & Ruan, X. Stronger role of four-phonon scattering than three phonon scattering in thermal conductivity of III-V semiconductors at room temperature. *Phys. Rev. B* **100**, 245203 (2019).
21. Cardona, M. Electron-phonon interaction in tetrahedral semiconductors. *Solid State Commun.* **133**, 3–18 (2005).
22. He, W. et al. High thermoelectric performance in low-cost $SnS_{0.91}Se_{0.09}$ crystals. *Science* **365**, 1418–1424 (2019).
23. Luo, Z. Z. et al. High figure of merit in gallium-doped nanostructured n-Type PbTe *x*GeTe with midgap states. *J. Am. Chem. Soc.* **141**, 16169–16177 (2019).
24. Yuan, C. et al. Modulating the thermal conductivity in hexagonal boron nitride via controlled boron isotope concentration. *Commun. Phys.* **2**, 1–8 (2019).
25. Simkin, M. & Mahan, G. Minimum thermal conductivity of superlattices. *Phys. Rev. Lett.* **84**, 927 (2000).
26. Li, C. W. et al. Orbitally driven giant phonon anharmonicity in SnSe. *Nat. Phys.* **11**, 1063–1069 (2015).
27. Zhu, Y. et al. Physical insights on the low lattice thermal conductivity of $AgInSe_2$. *Mater. Today Phys.* **19**, 100428 (2021).
28. Wei, B., Sun, Q., Li, C. & Hong. J. Phonon anharmonicity: a pertinent review of recent progress and perspective. *Sci. China-Phys. Mech. Astron.* https://doi.org/10.1007/s11433-021-1748-7 (2021).
29. Li, C. W. et al. Structural relationship between negative thermal expansion and quartic anharmonicity of cubic ScF_3. *Phys. Rev. Lett.* **107**, 195504 (2011).
30. Budai, J. D. et al. Metallization of vanadium dioxide driven by large phonon entropy. *Nature* **515**, 535–539 (2014).
31. Lee, C. H. et al. Low-lying optical phonon modes in the filled skutterudite $CeRu_4Sb_{12}$. *J. Phys. Soc. Jpn.* **75**, 123602 (2006).
32. Wei, B. et al. Giant anisotropic in-plane thermal conduction induced by anomalous phonons in nearly-equilaterally structured $PdSe_2$. Preprint at *arXiv* https://arxiv.org/abs/2107.07959 (2021).
33. Liu, H. et al. Anomalously suppressed thermal conduction by electron-phonon coupling in charge-density-wave tantalum disulfide. *Adv. Sci.* **7**, 1902071 (2020).
34. Hlinka, J. et al. Origin of the "Waterfall" effect in phonon dispersion of relaxor perovskites. *Phys. Rev. Lett.* **91**, 107602 (2003).
35. Li, C. W. et al. Phonon self-energy and origin of anomalous neutron scattering spectra in SnTe and PbTe thermoelectrics. *Phys. Rev. Lett.* **112**, 175501 (2014).
36. Mukhopadhyay, S. et al. The curious case of cuprous chloride: Giant thermal resistance and anharmonic quasiparticle spectra driven by dispersion nesting. *Phys. Rev. B* **96**, 100301(R) (2017).
37. Wei, B. et al. Low-temperature anharmonicity and the thermal conductivity of cesium iodide. *Phys. Rev. B* **99**, 184301 (2019).
38. Cowley, R. A. Anharmonic crystals. *Rep. Prog. Phys.* **31**, 123 (1968).
39. Feng, T. & Ruan, X. Prediction of spectral phonon mean free path and thermal conductivity with applications to thermoelectrics and thermal management: a review. *J. Nanomater.* **2014**, 1 (2014).
40. Balkanski, M., Wallis, R. & Haro, E. Anharmonic effects in light scattering due to optical phonons in silicon. *Phys. Rev. B* **28**, 1928 (1983).
41. Smith, H. L. et al. Temperature dependence of phonons in $FeGe_2$. *Phys. Rev. Mater.* **2**, 103602 (2018).
42. Brugger, K. Generalized Grüneisen parameters in the anisotropic Debye model. *Phys. Rev.* **137**, A1826 (1965).
43. Toellner, T., Alatas, A. & Said, A. Six-reflection meV-monochromator for synchrotron radiation. *J. Synchrotron Radiat.* **18**, 605–611 (2011).
44. Said, A. H., Sinn, H. & Divan, R. New developments in fabrication of high-energy resolution analyzers for inelastic X-ray spectroscopy. *J. Synchrotron Radiat.* **18**, 492–496 (2011).
45. Abernathy, D. L. et al. Design and operation of the wide angular-range chopper spectrometer ARCS at the Spallation Neutron Source. *Rev. Sci. Instrum.* **83**, 015114 (2012).
46. Arnold, O. et al. Mantid—data analysis and visualization package for neutron scattering and μ SR experiments. *Nucl. Instrum. Meth. A* **764**, 156–166 (2014).
47. Squires, G. L. *Introduction of the theory of thermal neutron scattering*, (Cambridge University Press, 1978).
48. Fåk, B. & Dorner, B. Phonon line shapes and excitation energies. *Physica B Condensed Matter* **234**, 1107–1108 (1997).
49. Kresse, G. & Furthmüller, J. Efficiency of ab-initio total energy calculations for metals and semiconductors using a plane-wave basis set. *Comput. Mater. Sci.* **6**, 15–50 (1996).
50. Togo, A., Oba, F. & Tanaka, I. First-principles calculations of the ferroelastic transition between rutile-type and CaCl2-type SiO2 at high pressures. *Phys. Rev. B* **78**, 134106 (2008).
51. Siegle, G. et al. Zone-boundary phonons in hexagonal and cubic GaN. *Phys. Rev. B.* **55**, 7000–7004 (1997).
52. Perlin, P. et al. Raman scattering and x-ray-absorption spectroscopy in gallium nitride under high pressure. *Phys. Rev. B.* **45**, 83–89 (1992).

Acknowledgements

The work at Beijing Institute of Technology is supported by the National Natural Science Foundation of China with Grant No. 11572040 and Beijing Natural Science Foundation (Grant No. Z190011). This work is supported by University of California, Riverside via Initial Complement. Theoretical calculations were performed using resources of the High-Performance Computing Center in University of California, Riverside. B.W. thanks the Joint PhD Program of Beijing Institute of Technology. INS measurements used resource at the SNS, a Department of Energy (DOE) Office of Science User Facility operated by the Oak Ridge National Laboratory. This research used resources of the APS, a U.S. Department of Energy (DOE) Office of Science User Facility, operated for the DOE Office of Science by Argonne National Laboratory under Contract No. DE-AC02-06CH11357.

Author contributions

C.L. conceived this project. B.W., J.H., and C.L. designed the experiments. B.W., Q.C., A.H.S., and C.L. performed the IXS measurements. B.W., Q.S., Y.S., D.A., and C.L. performed the INS measurements. B.W., C.L., and J.H. performed the theoretical calculation. B.W., Q.C., Q.S., J.H., and C.L. discussed the data. B.W., Q.C., J.H. and C.L. wrote the paper. All authors contributed to discussing the data and editing the paper.

Competing interests

The authors declare no competing interests.

Additional information

Supplementary information The online version contains supplementary material available at https://doi.org/10.1038/s42005-021-00727-9.

Correspondence and requests for materials should be addressed to Jiawang Hong or Chen Li.

Peer review information *Communications Physics* thanks Bijay Sahoo and the other, anonymous, reviewer(s) for their contribution to the peer review of this work. Peer reviewer reports are available.

Reprints and permission information is available at http://www.nature.com/reprints

Publisher's note Springer Nature remains neutral with regard to jurisdictional claims in published maps and institutional affiliations.